NASA Contractor Report 165745

THE STRUCTURE AND PROPERTIES OF DIFFUSION ASSISTED BONDED JOINTS IN 17-4 PH, TYPE 347, 15-5 PH AND NITRONIC 40 STAINLESS STEELS

D. A. Wigley

KENTRON INTERNATIONAL, INC.
Hampton Technical Center
Hampton, Virginia 23666

SUBCONTRACTOR:
THE UNIVERSITY OF SOUTHAMPTON
Department of Mechanical Engineering
Southampton, England

Contract NAS1-16000
July 1981

National Aeronautics and Space Administration

Langley Research Center
Hampton, Virginia 23665

The Structure and Properties of Diffusion Assisted Bonded Joints in 17-4 PH, Type 347, 15-5 PH and Nitronic 40 Stainless Steels

1. Introduction

A potentially attractive technique for the construction of aerodynamic models for use in cryogenic and conventional wind tunnels involves machining a network of open channels into the surface of a flat plate which is then bonded with a matching plate to form a network of closed passages within the monolithic block. The bond so formed has to be strong and tough, especially for cryogenic use, and the technique clean and precise enough to prevent the blockage of the channels or cross leakage between adjacent channels. Initial trials carried out by P. G. Sandefur and P. L. Lawing of NASA Langley Research Center demonstrated that diffusion assisted bonds can be formed in 17-4 PH, 15-5 PH, type 347, and Nitronic 40 using electrodeposited copper as the bonding agent.

In this report, we describe the use of a number of metallurgical techniques to examine the structure and properties of these bonds in the hope of: (a) understanding the mechanisms involved and (b) defining the parameters which must be controlled to produce consistent bonds. Conventional metallographic and electron microprobe analysis of sections cut through the bond line show most joints to contain both diffusion bonded and copper brazed regions. Porosity present in some samples has been correlated with grinding patterns on the original plate surface, while in other cases voids may be due to the Kirkendall effect.

Stereoscan examination of fracture surfaces created at 300 and 77K permits identification of the micromechanisms of fracture within the bonding layer and at its interface with the parent metal. 77K fracture surfaces generally show more indication of the original grain boundaries together with less deformation within the grains than is observed on 300K fracture surfaces.

Use of the stereoscan also permits clear identification of the unwetted areas that not only reduce bond strengths but also allow pressure leakage between adjacent passages.

Sections 2, 3, 4 and 5 of this report describe the use of these techniques on 17-4 PH, type 347, 15-5 PH and Nitronic 40 respectively, while section 6 details the results of indentation hardness and Charpy V-notch impact tests. Finally, in section 7 the results are discussed in terms of a postulated model for the bonding process and recommendations are made for the next stages in the investigation.

2. 17-4 PH Stainless Steel

Sections perpendicular to the bond line were cut from the sample provided by NASA and mounted, polished and etched for conventional metallographic examination. V-shaped pressure tapping channels were present in the bond line and it was found necessary to lap the cut face for a considerable period prior to final polishing in order to remove cutting debris that had been smeared into the channels. Figure 1a) is a low magnification view of the etched surface and it shows the nature and orientation of the large inclusions which had become aligned during the rolling stage of plate manufacture. Figure 1b) at x200 gives a good indication of the general nature of the bond line. It can be seen that between 50 and 70% of the bond area is formed from brazed regions in which a copper rich material fills the joint between the two 17-4 PH plates, while a further 20% of the bond line is formed from diffusion bonds between the 17-4 PH plates. Voids account for the remaining ~5% of the bond line and are readily indicated because etchant, and the alcohol used to remove it, continue to weep from the voids and stain the surrounding area. Also visible is a light etching region, more pronounced on the left hand side of the bond line, which we believe to be a copper rich diffusion zone. Figure 1c) at x600, shows how the copper infills between grains and also penetrates down adjacent grain boundaries to a limited extent. Figure 1d), at a magnification of x900, is rather near the resolution limit of optical microscopy but

it is possible to see that the copper rich phase in the joint appears to have cracks in it.

In Figure 1e) the electron-microprobe analyzer has been used to form a topographical image at x1800 of a region of the bond identified by the seven small craters which are microhardness indentations. The image is not, unfortunately, very clear but the bond line can be seen to pass from top center to bottom right of the picture. The microprobe analyser is also capable of forming images from the characteristic X-rays generated by different elements in the material and Figure 1f) shows such an image generated by copper K_α X-rays. The strong signal for the bond line stands out even above the rather high background caused by the ≈4% copper present in 17-4 P. H. stainless steel. Figure 1g) shows an image generated by nickel K_α X-rays. Again the background signal is high but it is possible to make out a nickel deficient region in the bond line itself, with a nickel enhanced region on each side of the bond. Upon investigation, it has been learned that the shop which carried out the electroplating followed the standard commercial practice of laying down a flash coat of nickel prior to the copper coating thus accounting for the nickel rich area. Figure 1h) is a chromium K_α X-ray image showing chromium deficiency in the bond line.

A second specimen, 16mm long × 10mm wide × 2mm thick was cut so that the bond line was located at the mid point of the span and in the through thickness direction. This specimen was then broken in 3 point bend and one fracture surface mounted for observation in a Cambridge Stereoscan scanning electron microscope. Figure 2a) shows a low magnification (x35) view of the fracture surface with the right hand edge visible: the dark streaks that run from top to bottom are unbonded areas. Figure 2b), magnification x140, has two boxes drawn on it to identify the areas selected for more detailed examination. The area at the bottom left of Figure 2b) contains an unbonded region and this is shown in Figures 2c), d) and e) at magnifications of x350, x700 and x1400 respectively. It can be seen that the unbounded grains have a smooth, rounded appearance, and that the grain boundaries are quite deeply etched, probably by the molten copper before it retreated from these regions.

Figures 2f), g) and h) show the second area indicated in Figure 2b) at the magnifications of x350, x700 and x1400 respectively. Although some small unbonded grains are visible, the salient features are of a series of ridges and craters many of which have second phase particles within them. The ridges are interpreted as being formed by the ductile shear failure of the copper rich regions of the bond, while the craters containing second phase particles are characteristic of the so-called "ductile-dimple" mode of failure. The particles are usually irregular in nature and in some cases clearly cracked.

In an attempt to identify the nature and origin of these particles the microprobe analyser was again used even though the fracture surface was not completely flat. (The irregular nature of the surface causes complications in analysing the X-ray signals due to absorption by the high spots of X-rays originating from the lower regions). Results are shown in the series of photographs of Figure 3. In a) a topographical image at magnification x1000 shows "ductile-dimple" features similar to those in the stereoscan photograph, 2h), at x1400. In b), c) and d), K_{α} X-ray images are shown for Silicon, Calcium and Chlorine respectively. As can be seen, it is possible to associate strong silicon and calcium X-ray signals with the precipitates marked B and C in Figure 3a), as well as a weaker chlorine signal. If the plating solutions used to prepare the copper electrodeposit were very impure, it might be possible to argue that these precipitates could be associated with the copper. However, comparison with the chromium and copper X-ray images shown in e) and f) show that these silicon and calcium rich precipitates occur in both copper rich and copper deficient regions. Even more striking, however, is the precipitate marked A in Figure 3a) which in g) and h) can be seen to be associated unmistakably with strong sulphur and manganese signals, hence identifying A as a manganese sulphide inclusion. As manganese sulphide can only be from the parent metal, this is a clear indication that ductile fracture of a diffusion bonded region has taken place around precipitate A. It is possible that the other inclusions originate from the parent metal but, as yet, no clear identification is possible.

A third specimen, similar in size and type to the second, was pre-cooled to 77K with liquid nitrogen and then rapidly broken in an impact bend mode before the temperature rose significantly. It too was mounted for stereoscan examination of the fracture surface and the results are shown in Figure 4. Very little detail can be observed in Figure 4a) but it does serve to locate the region, at its center, which is subsequently examined in more detail in b), c) and d) at magnifications of x350, x700 and x3500 respectively. A second typical region is shown in e) and f) at a magnification of x700 and x1400 and this illustrates clearly the basically intergranular nature of the fracture: Figures 4g) and h) show further representative areas of the fracture surface. The principal differences between the low and ambient temperature fracture modes may be illustrated by comparing Figures 2d) and g) (300K fracture, x700) with Figures 4c), e) and g) (77K fracture, x700 magnification). Grain boundaries in Figure 4 (77K) are generally straighter and less distorted than in Figure 2 (300K). The inclusions at 77K are more rounded and less cracked than at 300K, and there is very much more fine detail visible on the 77K fracture surfaces. For example, both Figure 4f) and 4h) show very fine "ductile-dimple" zones as well as areas where parallel bands of low ridges are visible, whereas such detail is absent in Figures 2e) and 2h) even though they were taken at the same magnification.

Thus, to summarise briefly, the joints formed by diffusion assisted bonding of copper in 17-4 P. H. stainless steel are a mixture of brazed and diffusion bonded regions, with some voids. Fracture surfaces formed at both 300 and 77K show that the microscopic failure modes are basically ductile in nature, but that there is less deformation in the bond zone at the lower temperature. In this respect, the behaviour of the bond reflects that of 17-4 P. H. stainless itself which suffers from a loss of toughness at low temperatures.

3. Type 347 Stainless Steel

Sections perpendicular to the bond line were cut from the sample provided and mounted, polished and etched for metallographic examination.

It was, however, difficult to achieve a good, stain-free, etched surface because the polishing fluid and etchant "wept" copiously from the bond line. Figure 5a) shows some evidence of this staining even after prolonged cleaning: it also reveals the grain structure to be as expected for a 300 series stainless steel, with many parallel-sided annealing twins visible within the main grain. Figure 5b) shows a scanning electron image of the bond line at a magnification of x500, while 5c) presents the copper K_α X-ray image of the same region. Also shown is the intensity of the copper X-ray signal as it is scanned across the bond line at the position indicated by the dark horizontal line visible in Figure 5b) and marked AA' in 5c). This line traverses one of the diffusion bonded portions of the interface and the trace shows the copper diffusion zone to have a width of approximately 40 microns ($\sim 1.6 \times 10^{-3}$ inches). For comparison the original copper plated layer was stated by NASA to have a thickness of ~5 microns (2×10^{-4} inches).

A second specimen similar to that used for the 17-4 P. H. tests (16 × 10 × 2mm) was broken in 3 point bending to expose a fracture surface. Little effort was required and there was virtually no plastic deformation prior to failure. Figure 5d) gives a low power view of the fracture surface and shows the alternating light and dark bands indicating bonded and unbonded regions respectively. These are more clearly visible in Figures 5e), g) and h) at magnifications of x140, x350 and x1400 respectively. The x1400 view in h) indicates the "ductile-dimple" nature of failure in the bonded region, and also a series of "tide marks" on the surface of the unbonded area. As at least 50% of the fracture surface is unbonded, the poor strength and high porosity of the joint can be readily understood. Nevertheless, strong bonds must have been formed in some areas because the hole visible in Figures 5e) and f) indicates that in this region the bond strength exceeded that of the interface between the parent metal and an inclusion or "stringer" (probably manganese sulphide) nearby. The ductile nature of this localised failure is demonstrated by the presence of "ductile-dimples" as shown in 5f).

The possible significance of the "tide marks" on the surface of the unbonded grains will be considered further in Section 6 when possible

models for bond formation are discussed. No low temperature tests were carried out on type 347 stainless steel because it was considered that this sample was unrepresentative of the quality of bonds that could be produced in this material.

4. 15-5 P. H. Stainless Steel

Due to its ready availability, good stability during heat treatment and machining, and its reputation for taking a very good surface finish, 15-5 P. H. stainless steel is an attractive candidate material for constructing a wind tunnel model. Although its cryogenic fracture toughness values are not high enough for use in the large cryogenic tunnels, handbook values indicate that it is above the minimum set for use in a small, 2-D airfoil tunnel at the H 1150-M condition. Since great accuracy in contour and good surface finish are very desirable in 2-D airfoil testing, 15-5 P. H. is an important candidate for this study.

As with the two previous materials, samples were cut, polished and etched for metallographic examination, and once again there was considerable "weeping" from voids in the bond line. Figure 6a) shows the appearance of an etched surface at x200, the grain structure being very similar to that given in Figure 1b) for 17-4 P. H. stainless. Figure 6b) illustrates the compositional image obtained from the microprobe analyser at a magnification of x1500, while 6c) gives the corresponding copper K_α X-ray image. Figure 6d) shows two traces for the intensity of the copper X-ray signal as the beam is scanned along the lines AA' and BB'. The line AA' passes through a copper rich brazed region and a very strong signal is generated, so strong in fact that the peak of the signal is lost off the top of Figure 6d). The line BB' traverses a diffusion-bonded region of the joint and the copper signal shows a much lower peak intensity; the width of the diffusion zone is, however, substantially the same for both traces, indicating that similar diffusion mechanisms are involved in the copper-rich and copper-depleted zones.

Figure 6e) gives a strong indication of the probable cause of the "weepage" from the voids in the bond line of the polished specimen. Once again the dark areas correspond to the unbonded regions and the light to the bonded. The overall pattern of light and dark areas appears very similar to that formed by grinding a flat surface, and we believe that the quality of the ground finish left on the surface prior to electroplating plays a crucial role in determining the quality of any subsequent bond, particularly in hard materials such as the precipitation hardened stainless steels. Thus far, simple commercial grinding has been employed and the grinding quality has not been closely monitored. The quality of finish necessary to generate a bond in a given material is a subject for future research.

A second 15-5 P. H. specimen, similar in size and form to that used for 17-4 P. H. and type 347, was broken in 3 point bending to expose a fracture surface of the bonded joint. Figure 6f) gives a low magnification view of the full depth of the exposed surface and it is immediately apparent that in this material too there are large unbonded areas from which etchant can weep and stain a polished surface such as in Figure 6a). Figures 6g) and 6h) show both bonded and unbonded areas at magnifications of x350 and x1400 respectively. The general appearance of the fracture surface in the bonded region is of a fine scale "ductile-dimple" nature superimposed on a basically intergranular type of failure. The grain boundaries remain relatively straight and undistorted and, although this fracture surface was created at 300K, its characteristics are much more in common with that shown in the stereoscan pictures of Figure 4 taken from a 77K fracture surface in 17-4 P. H. stainless, than with the 300K fracture surfaces in 17-4 P. H. shown in Figure 2. Thus it appears that failure at 300K in 15-5 P. H. stainless is of a rather low energy, intergranular nature and this must, unfortunately, restrict the potential use of this type of bonded joint in 15-5 P. H. stainless if this sample is typical of the material, and if the bond in question is highly loaded.

Finally, the high magnification view of the unbonded area visible in Figure 6b) illustrates once again the "tide-marks" noted in previous

specimens. The high angle of tilt effectively obtained at the top left hand corner of Figure 6h) allows these "tide-marks" to be seen almost in profile and their step-like nature is illustrated.

5. Nitronic 40

This material has been chosen for construction of the pilot model for use in the National Transonic Facility because it has the optimum combination of strength and toughness at the low operating temperatures of a cryogenic wind tunnel. The ability to form diffusion assisted brazed joints would therefore be an additional, very welcome, bonus if the technique could be proven.

Figures 7a), b), c) and d) show micrographs obtained from a polished and etched section of the Nitronic 40 sample supplied by NASA. The low power view of 7a) illustrates the general nature of the grain structure with its characteristic annealing twins similar in many respects to that shown in Figure 5a) for type 347 stainless steel, but with a much larger grain size in Nitronic 40. Bands of large inclusions can be seen running parallel to the bond line, indicating that the original plate rolling direction was also in this direction. The size of the inclusions can be judged by comparing Figure 7c) through h) at a magnification of x4750. The copper X-ray image of magnification. There was little or no "weeping" from the polished and etched surface and few, if any, voids are present. Indeed, the section shown at a magnification of x900 in Figure 7d) indicates that the copper-rich phase fits tightly into the boundary between the two plates and does not appear to crack at break-up. The results of microprobe analysis on this sample are shown in Figures 7e) through h) at a magnification of x4750. The copper X-ray image of 7f) shows only limited diffusion into the parent metal, while the manganese X-ray image of 7g) indicates that there is manganese enhancement in the copper rich region of the bond. As the copper electrodeposit contained no manganese, this must have occurred by diffusion of manganese from the Nitronic 40 into

the copper. The nickel X-ray image of 7h) indicates a minor nickel enrichment adjacent to the copper bond line, which may have been due to the provision of a thin nickel "flash coat" by the electroplaters.

The photographs illustrated in Figure 8 show the results of a very significant experiment in which one side of a slice of Nitronic 40, 20mm long × 10mm wide × 2mm deep, with a through thickness bond at its mid span, was highly polished to a 1 micron diamond finish. This specimen was then bent through a 60^{o} angle in 3 point bending with the polished surface put under tension. Only a limited degree of bond failure occurred and this was at the specimen edge as shown in 8a). Figures 8b) and 8c) show the tip of this crack at magnifications of x80 and x800 respectively and illustrate the very ductile, tearing nature of the failure. Figures 8d) and 8e) portray a smaller region of debonding further in from the specimen edge at magnifications of x200 and x400 respectively.

In most of these photographs many slip lines are visible, all having the same parallel orientation within a grain, but whose directions change at the grain boundaries. These are indications of the crystallographic nature of slip in materials which only occurs on certain planes and in specific directions. Cross slip is visible in some grains, e.g. center left in Figure 8e), where two intersecting slip systems are in operation within the same grain. These markings only appear as a result of plastic deformation of the metal and they are, therefore, an infallible indication that stresses in these grains have exceeded the local yield stress. With this in mind, examination of the photographs of a typical intact region of the bond line, Figures 8f), g) and h), permits an interpretation of the characteristics of the copper-rich phase in the boundary. Slip lines are clearly visible within the copper-rich phase which must therefore be ductile and which must also be strong enough to remain unbroken at stresses large enough to cause yield and plastic deformation of the adjacent grains of Nitronic 40.

Thus, when tested at room temperature, the bond formed by diffusion assisted brazing of copper in Nitronic 40 is strong and ductile enough to

permit yield and very significant plastic deformation of the Nitronic 40 itself.

A further, similar specimen was tested to failure in 3-point bending at room temperature and one fracture surface was mounted for stereoscan examination. The results are illustrated in Figure 9. The low magnification view of Figure 9a) shows that although failure was predominantly in the bond line, a large hole had been pulled out of the parent metal on the center of Figure 9a). This area is seen in more detail at the top of Figure 9b) and at still higher magnification (x300) in 9g), while the x3000 magnification view of Figure 9h) shows the classic "ductile-dimple" nature of the fracture surface in the parent metal. Recalling the large inclusions seen in the metallographic sections of Figures 7a) and 7c), the most likely explanation for this feature is that the strength of the inclusion - matrix bond in the Nitronic 40 was lower than that of the bonded joint nearby and so the crack propagated away from the bond and took the line of least resistance down the inclusions.

Figures 9e) and f) show the surface of the fracture where it had taken place in the bond line, the x1200 magnification view of Figure 9f) showing not only the ductile ridges where final shear failure occurred, but also slip lines in the grains between the shear ridges.

The region immediately beneath the pulled out area is essentially unbonded and is shown in more detail in Figure 9e). Parallel slip lines are visible on the surface of the unbonded grains but care has to be taken in their interpretation in order to avoid confusion with the "tide-mark" lines already noticed in the previous materials. Indeed, interpretation of the markings visible on the unwetted grains in Figure 9d), which is from a different area of the fracture surface, is ambiguous and it is difficult to be sure whether they are slip lines or "tide-marks."

The details of Charpy impact tests on the bonded materials will be considered in detail in the next section, but the results of stereoscan

examination of the fracture surface of a Nitronic 40 Charpy bar broken at 77K are more appropriately considered here. Figure 10a) gives a view of one edge of the fracture surface, and the parallel sided strip running from the center of the specimen to the middle of the left hand edge is a manufactured groove representative of the wind tunnel model pressure channels that happened to intersect the bond line at this point. The exposed fracture surface of the bond lies above and to the right of this channel. Figure 10b) shows this fractured region at a magnification of x70 and the center of this region is in turn shown in 10c) at x350. This illustrates a typically representative area of fracture with much evidence of ductile failure on a fine scale, such as the fishscale like ridges shown in detail at x1400 in 10d), as well as the large includion arrowed at A (10c)) and the group of small, angular inclusions arrowed at B. A second, equally typical region, is shown in Figures 10e) and f) at x350 and x1400 respectively. The fine structure is more ridge-like, as if microscopic shear lips were aligned parallel to each other, and in e) there is a large hole which looks as if it once held an inclusion. Finally, Figures 10g) and h) show areas in which the grains are partially unwetted, and two intersecting systems of parallel slip lines are visible in these areas. The other striking feature in these photographs is of the clear, angular, undistorted form of the inclusions, indicating that the inclusion-matrix bond broke easily without unduly deforming the inclusions.

Comparison between Figures 9 and 10 once again indicates the finer scale of the features on the fracture surface of specimens broken at low temperatures. Nevertheless the fracture is still ductile in nature and the bond is strong and reasonably tough, although probably not as tough as at room temperature.

6. Macrohardness and Charpy Impact Tests

Macrohardness measurements give a simple and rapid indication of the hardness, and by implication, tensile strength, of a material. The four types of material under investigation were therefore tested using a Vickers Diamond

Pyramid indenter with a 20 kg load and the results obtained are as given in Table 1. (The VPN in Table 1 refers to Vickers Pyramid Number.)

Table 1

Material	VPN	Equiv. Tensile Strength		Hardness expected for indicated temper.					
		(MPa)	(KSI)	H900F	H1025F	H1075F	H1100F	H1150F	H1150M
17-4 P.H.	390	1270	185	412	381	350	-	316	-
15-5 P.H.	396	1290	187	395	327	303	291	281	239
347	143	495	72	-	-	-	-	-	-
Nitronic 40	182	615	89	-	-	-	-	-	-

Also shown are the hardness values to be expected from the various precipitation hardening heat-treatments carried out on 17-4 and 15-5 grades of stainless steel. It is readily apparent that the hardness values obtained experimentally indicate that both materials are in the fully hardened condition which would give them minimum toughness and make them less suitable for cryogenic applications.

Nitronic 40 and type 347 stainless steel have significantly lower hardnesses than the precipitation hardened varieties, the greater hardness of Nitronic 40 reflecting its known superior tensile strength when compared to type 347.

Standard size Charpy V-notch impact test bars were prepared from bonded samples of 347, 15-5 P. H. and Nitronic 40: there was insufficient material available to prepare Charpy bars from the 17-4 P. H. sample. Due to a misunderstanding in our workshops, 90^{o} notches were cut into the bars instead of the standard 45^{o} notch, so the impact energies recorded experimentally are probably slightly high due to the smaller stress concentration factor of the blunter notch; nevertheless, the trends shown are correct.

Two types of specimen were made with notch geometries as indicated in Figure 12. Through notch specimens, subsequently referred to as T types, had the notch cut perpendicular to the axis of the bond line, Figure 12a). Surface notched specimens, S-types, had the notch cut such that its root was parallel to the bond plane as indicated in Figure 12b). As the bond line will tend to delaminate and blunt a crack that runs into it, the S-type samples would be expected to give higher impact energies than the T-types. The results obtained from tests at 300K and 77K are as given in Table 2.

Table 2

Material	Test Temperature(K)	Specimen Number	Specimen Type	Impact Energy (ft.lb)	Impact Energy (joules)
Nitronic 40	300	1	T	96	71
"	300	2	S	107	79
"	77	3	T	41	30
"	77	4	S	93	68
Type 347	300	1	T	66	49
"	300	2	S	83	61
"	77	3	T	50	37
"	77	4	S	107	79
15-5 P.H.	300	1	T	19	14
"	300	2	S	72	53
"	77	3	T	2.2	1.6
"	77	4	S	1.8	1.3

The fracture surfaces of all the Charpy bars tested are shown in Figure 11a) to f) and the differences between T and S type samples are readily apparent. In Nitronic 40 and type 347 at both 300K and 77K the S-type

specimens delaminated and blunted the crack sufficiently to prevent fracture of the underlying half of the bar, and even in 15-5 P. H. at 300K it increased the impact energy significantly in comparison with the T-types. Two basic principles may be illustrated by these examples. Firstly, the most realistic, if severe, results are obtained from specimens with through thickness notches. Secondly, additional toughness can be achieved in practical situations if one or more bonded joints can be placed perpendicular to the most likely crack propagation paths.

7. Discussion, Conclusions and Recommendations

In order to rationalize the above results, it is necessary to have a working model of the processes that occur during vacuum brazing. One possible model is shown in Figure 13. No surfaces are truly flat and contact between two surfaces takes place at their asperities. Furthermore, a well applied electrodeposited layer will be deposited evenly over both hills and valleys. This situation is depicted schematically in Figure 13a) where contact occurs between the high spots of the coated surfaces. A small amount of local deformation might occur at the peaks, but this is unlikely to be significant in view of the low pressures applied. When the specimen is heated in vacuum it is believed that at temperatures above ~1000° C (1800° F) the protective oxide layer is broken down and when the copper melts at 1083° C (1981° F), it is able to "wet" the surface of the stainless steel. If the surface roughness is low, or the amount of copper applied is large enough, the whole of the gap between the two surfaces will be filled with molten copper and if the specimen were cooled from this state a void-free, fully-brazed joint would be formed, Figure 13b). If, however, the specimen were held at the high temperatures used in the process, ~1180° C (2150° F), copper atoms would diffuse away from the joint, down grain boundaries or into the grains themselves. The asperities on the stainless steel surface would come into contact and diffusion bonds form across the joint at these points, the process being assisted by dissolution of the high spots by molten copper. Other things being equal, the greater the proportion of the joint bridged by diffusion bonds, the stronger it would become.

Eventually, however, the diffusion of copper away from the bond zone will start to create small voids in the brazed regions as indicated in Figure 13c) because there will not now be enough copper left to fill the joint completely. If even longer holding times are maintained, the continual diffusion of copper atoms into the grains, or more probably down the grain boundaries, will lead to the enlargement of these voids and the effective loss of the brazed joint. The residual molten copper will be drawn by capillary action into the narrow gaps at the grain boundaries and so leave the valleys free of copper. As molten copper dissolves the surface of the stainless steel, it is possible that the "tide-marks" noted on several of the unbonded areas of the samples are witness marks left behind as the copper retreated from these regions. Alternatively they may be indications of "thermal etching" of the uncoated surface. Not only do these voids cause the fluid entrapment that gave staining problems with the metallographic specimens, but they could form cross leaks between closely spaced pressure passages and they could also degrade the surface finish of aerofoil models where the joint line intersected the surface.

If this model is correct, it would suggest that the optimum joint would be obtained from a mixture of brazed and diffusion bonded regions that was completely void free. Excessive holding times and high temperatures should, therefore, be avoided as they encourage void formation and the grain boundary migration of copper which is likely to favour an intergranular fracture mode.

In the 15-5 P. H. and 347 samples, it was noted that the pattern of bonded and unbonded regions was highly suggestive of the ground finish of the original plates of stainless steel. If it is not possible to improve this finish, thought must be given to applying thicker layers of electrodeposited copper or even copper foils to give an enhanced gap-filling capability. However, the need to prevent blockage of the pressure channels puts an upper limit on the thickness of deposit or foil that could be utilised.

The outstanding need is, therefore, for a systematic evaluation of the effects of changing, under controlled conditions, the various parameters

that determine the characteristics of the bond. The most important of these parameters are:

- the filler metal or alloy,
- the time spent at temperatures above the melting point of the filler metal used,
- the temperature range over which the sample is heated, held and cooled,
- the pressure applied,
- the surface roughness of the steel plates,
- the thickness and nature of the electrodeposit or thin film of filler metal,
- the atmosphere or level of vacuum needed to remove the oxide on the stainless steel surface.

Ideally, all these parameters would need to be varied for each type of stainless steel under consideration, and this could be a very time-consuming project. Some simplification could be achieved by grouping together Nitronic 40 and type 347 stainless steels as both have the inherent toughness required for use in a cryogenic wind tunnel. In view of the very high quality bond already achieved with Nitronic 40, taken together with its superior strength and toughness, there seems little point in proceeding further with type 347 at this stage.

The situation with the precipitation hardened grades is more complex. The results outlined in this report seem to favour 17-4 P. H., but it is possible that the 15-5 P. H. sample was untypical. Furthermore, although neither alloy is really tough enough for cryogenic use, the slightly lower strength of 15-5 should make it slightly tougher than 17-4. Priority between 15-5 and 17-4 will therefore, have to be decided by NASA by taking into consideration other factors such as machinability or satisfactory experience of working with 15-5 P.H. in models for conventional wind tunnels.

The size of the samples supplied so far has restricted the tests that can be carried out on the mechanical properties of the diffusion bond. In particular, the plates have been too thin to allow tensile specimens to be machined large enough to fit in any of our test rigs. A limited amount of data could, however, be obtained using small 3 point bend test samples in a specially developed facility, and it is suggested that such tests should be carried out as part of the next phase of this programme. Nevertheless, thicker plates of stainless steel should also be used in the production of future test samples so that tensile tests can be carried out to cross-check the results obtained in the 3 point bend tests.

FIG.1: 17/4 P.H. STAINLESS STEEL, POLISHED AND ETCHED SECTIONS

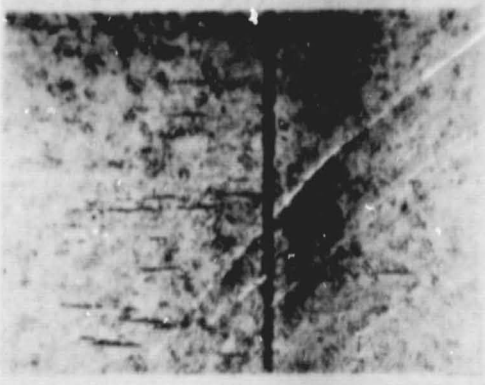

a) Metallographic, x 40

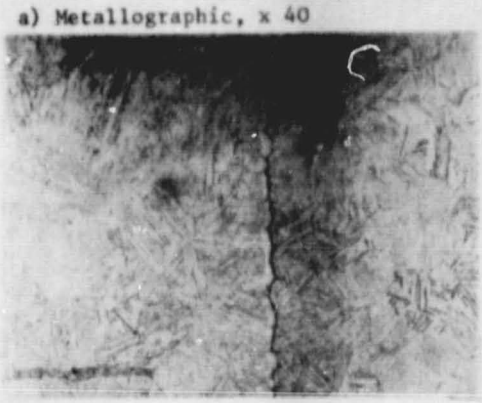

b) Metallographic, x 200

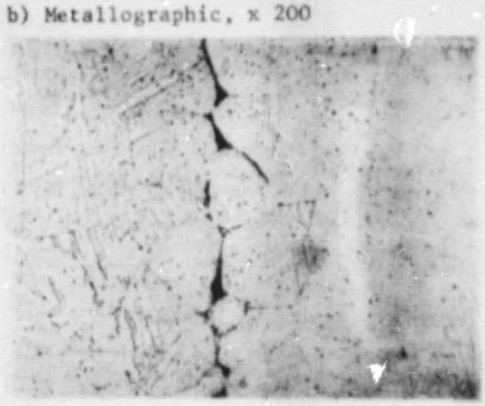

c) Metallographic, x 600

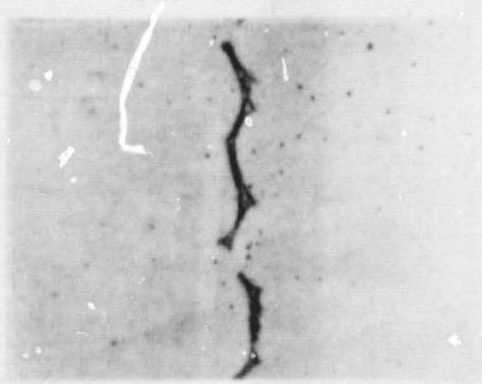

d) Metallographic, x 900

e) Microprobe, x 1800, Topographical

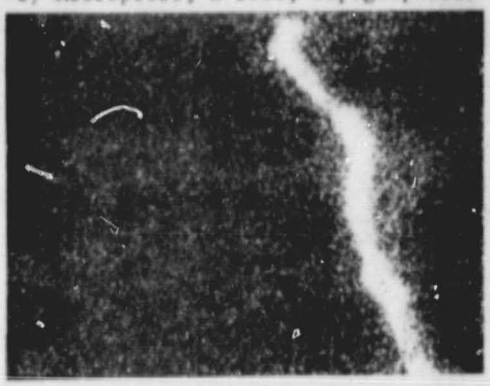

f) Microprobe, x 1800, Copper X-ray

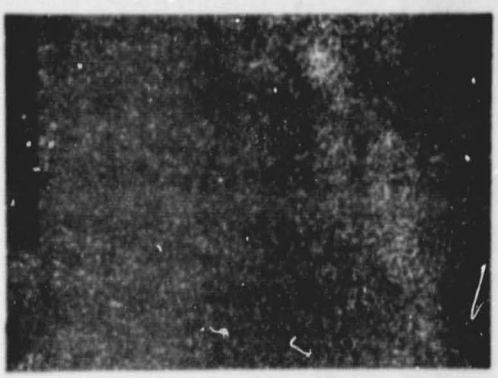

g) Microprobe, x 1800, Nickel X-ray

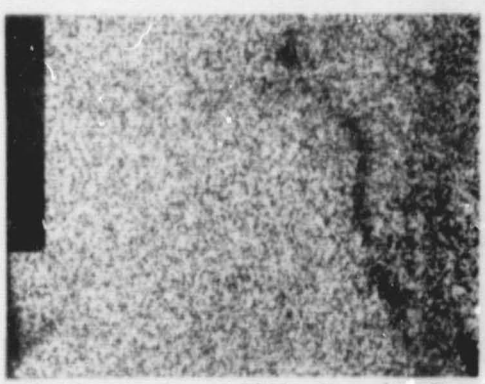

h) Microprobe, x 1800, Chromium X-ray

FIG.2: 17/4 P.H. STAINLESS STEEL, 300K, 3Pt BEND FRACTURE SURFACE

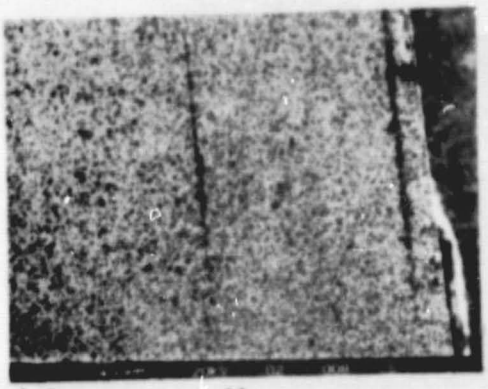

a) Stereoscan, x 35

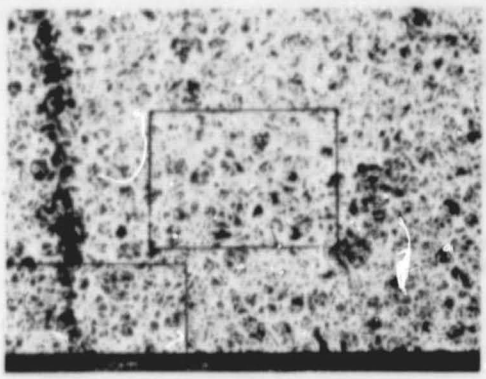

b) Stereoscan, x 140

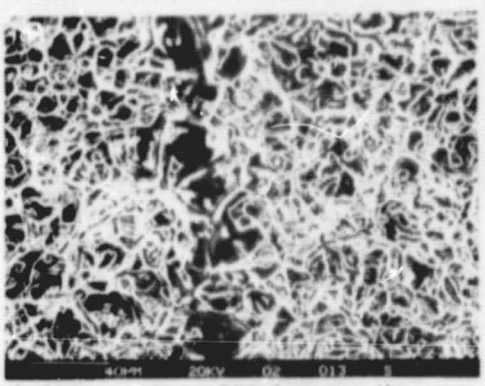

c) Stereoscan, x 350 (unwetted)

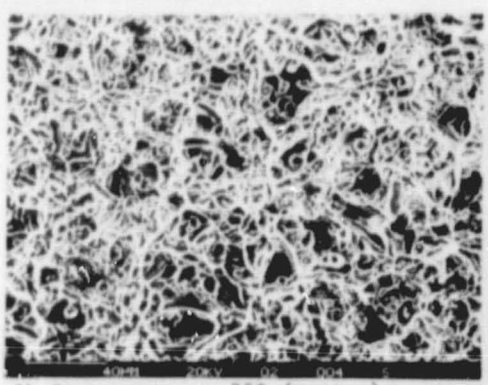

f) Stereoscan, x 350 (centre)

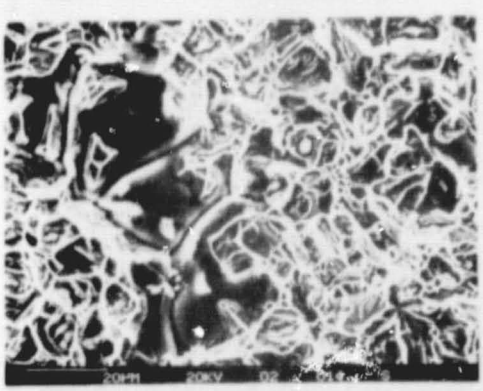

d) Stereoscan, x 700 (unwetted)

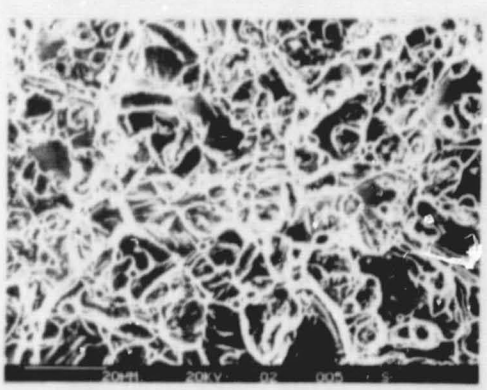

g) Stereoscan, x 700 (centre)

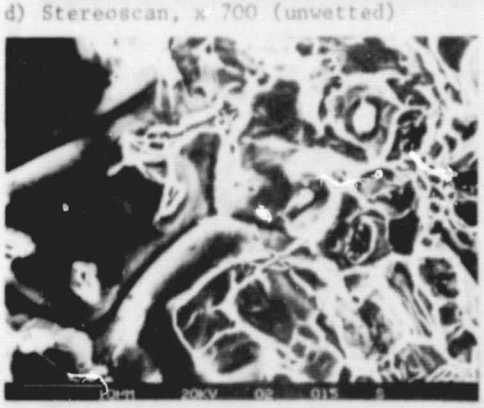

e) Stereoscan, x 1400 (unwetted)

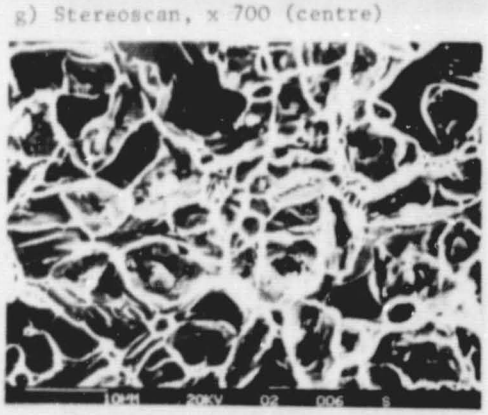

h) Stereoscan, x 1400 (centre)

FIG.3: 17/4 P.H. STAINLESS STEEL, 300K, 3pt BEND FRACTURE SURFACE

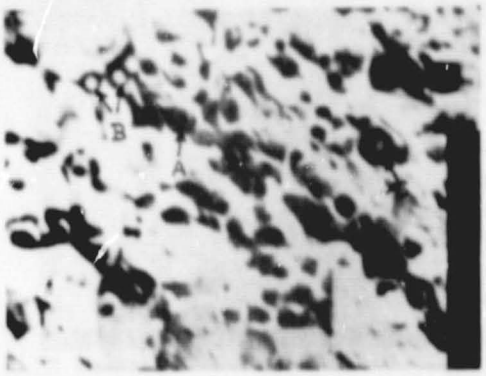

a) Microprobe, x 1000, Topographical

b) Microprobe, x 1000, Silicon X-ray

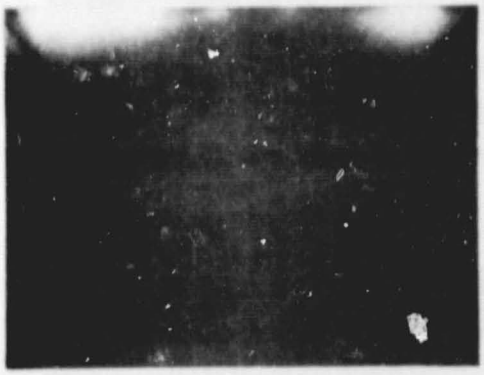

c) Microprobe, x 1000, Calcium X-ray

d) Microprobe, x 1000, Chlorine X-ray

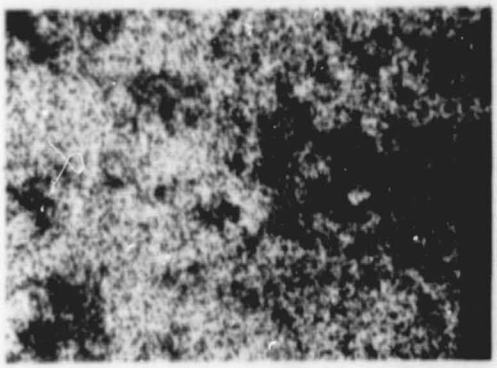

e) Microprobe, x 1000, Chromium X-ray

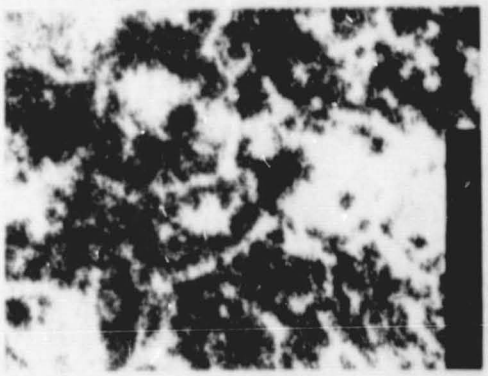

f) Microprobe, x 1000, Copper X-ray

g) Microprobe, x 1000, Sulphur X-ray

h) Microprobe, x 1000, Manganese X-ray

FIG.4: 17/4 P.H. STAINLESS STEEL, 77K IMPACT BEND FRACTURE SURFACE

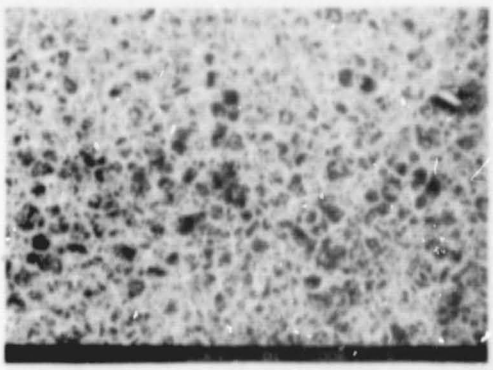

a) Stereoscan, x 140

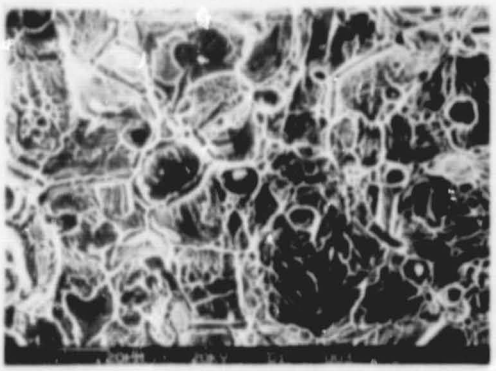

e) Stereoscan, x 700 (2nd area)

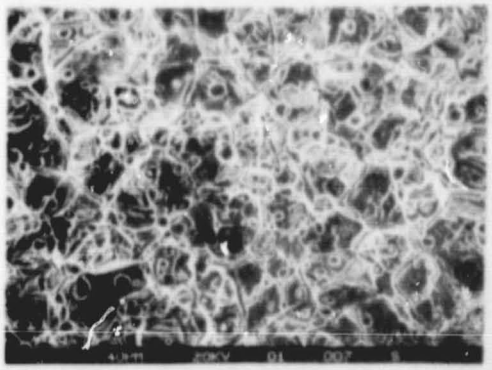

b) Stereoscan, x 350

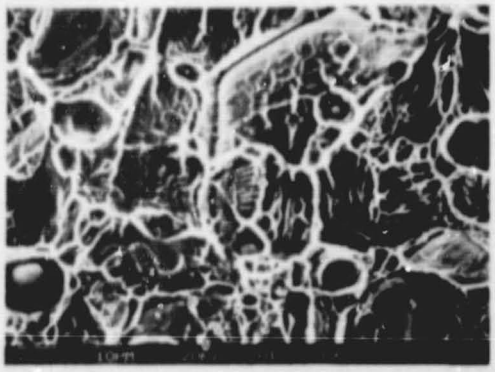

f) Stereoscan, x 1400 (2nd area)

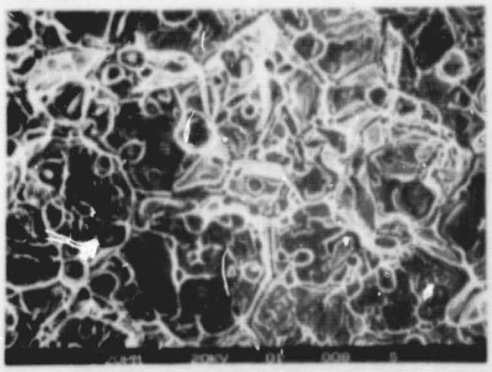

c) Stereoscan, x 700

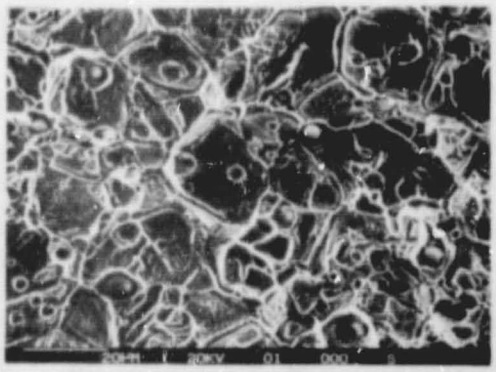

g) Stereoscan, x 700 (3rd area)

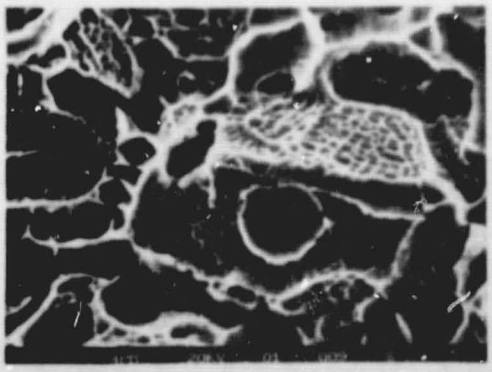

d) Stereoscan, x 3500

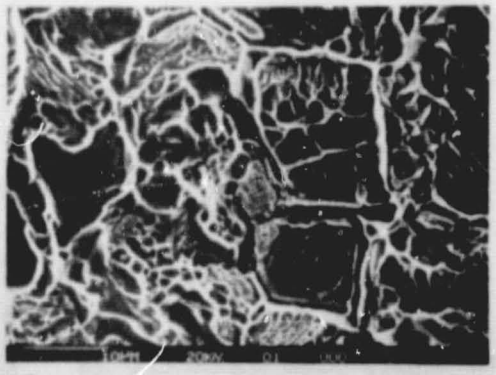

h) Stereoscan, x 1400 (4th area)

FIG.5: TYPE 347 STAINLESS STEEL, SECTIONS AND 300K FRACTURE SURFACE

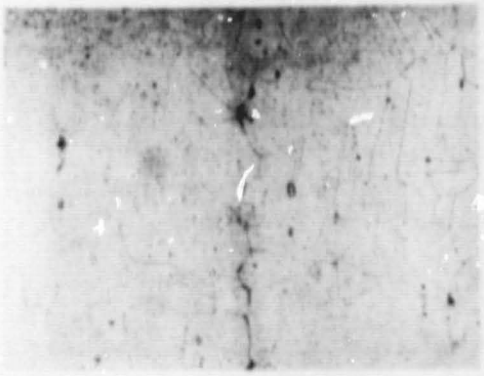

a) Metallographic section, x 200

b) Microprobe, x 500, Scanning Electron Image

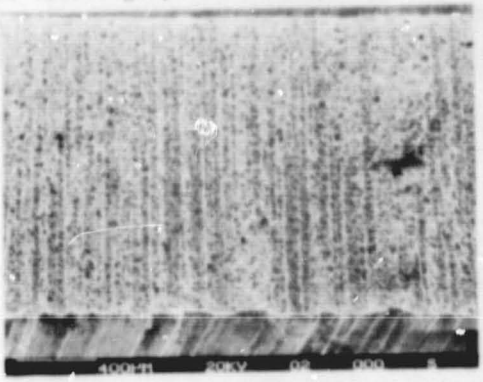

d) Stereoscan, x 35

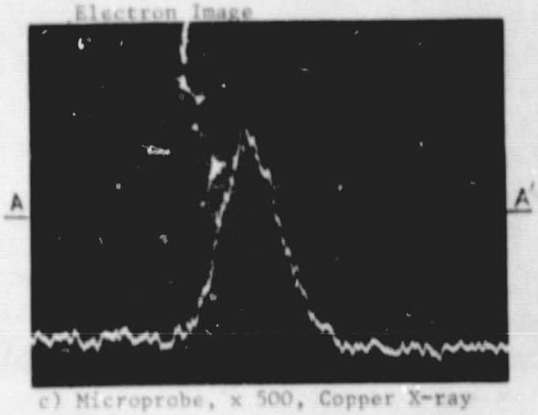

c) Microprobe, x 500, Copper X-ray and trace

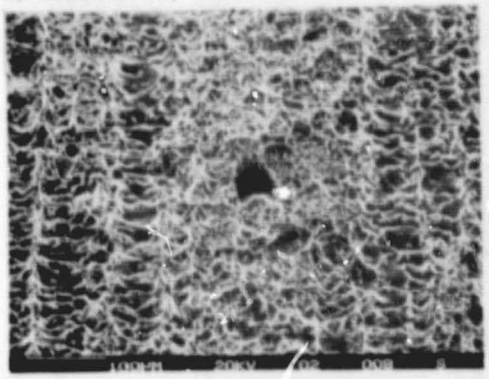

e) Stereoscan, x 140

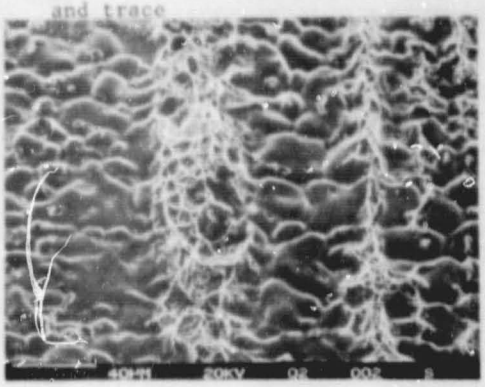

g) Stereoscan, x 350 (2nd area)

f) Stereoscan, x 1400

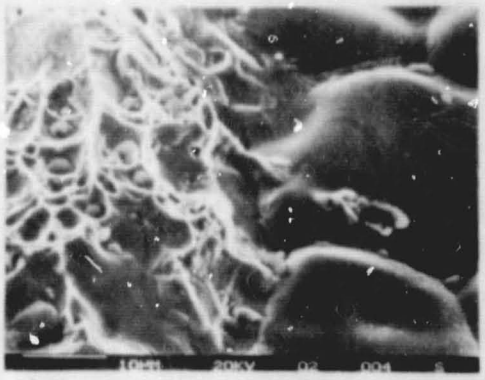

h) Stereoscan, x 1400 (2nd area)

FIG.6: 15/5 P.H. STAINLESS STEEL, SECTIONS AND 300K FRACTURE SURFACE

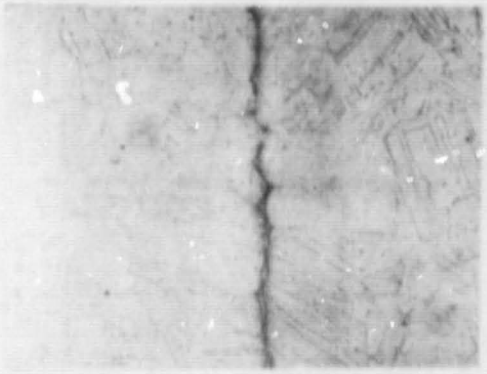

a) Metallographic section, x 200

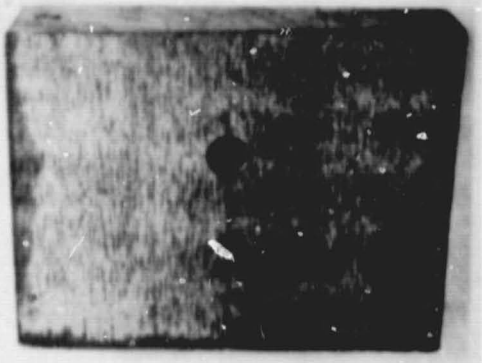

e) Fracture surface, x 1

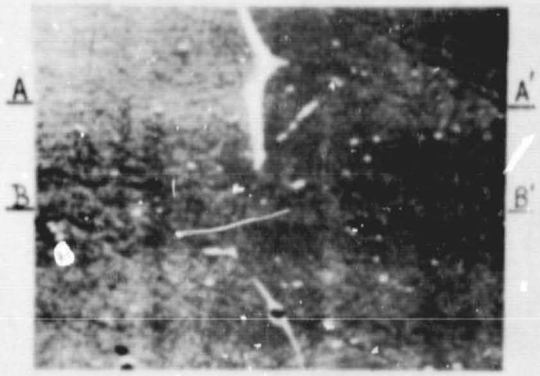

b) Microprobe, x 1500, Compositional

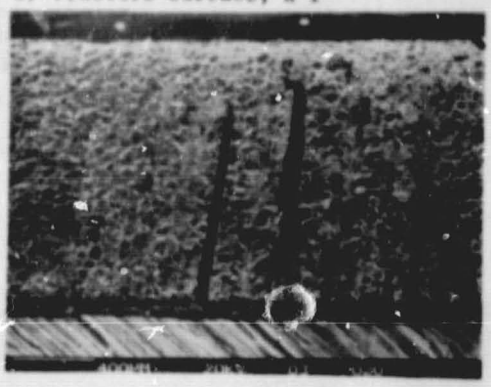

f) Stereoscan, x 35

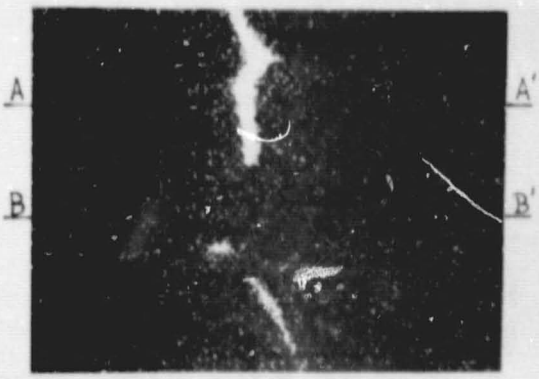

c) Microprobe, x 1500, Copper X-ray

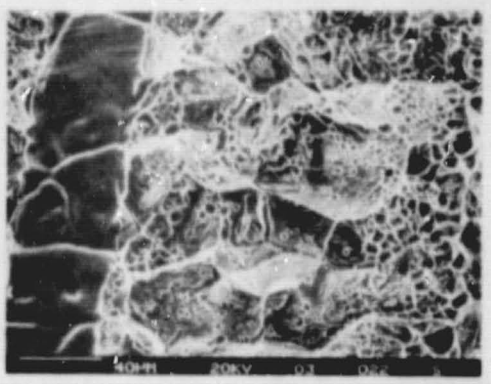

g) Stereoscan, x 350

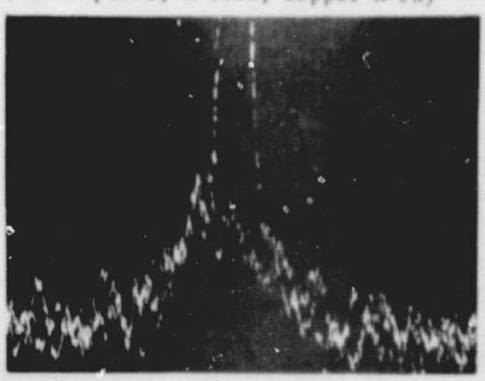

d) Microprobe, x 1500, Copper X-ray traces

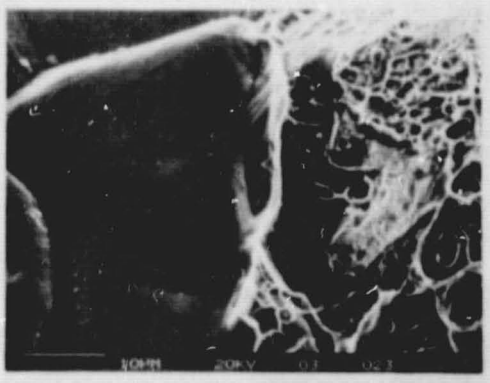

h) Stereoscan, x 1400

FIG.7: NITRONIC 40 STAINLESS STEEL, POLISHED AND ETCHED SECTIONS

a) Metallographic, x 40

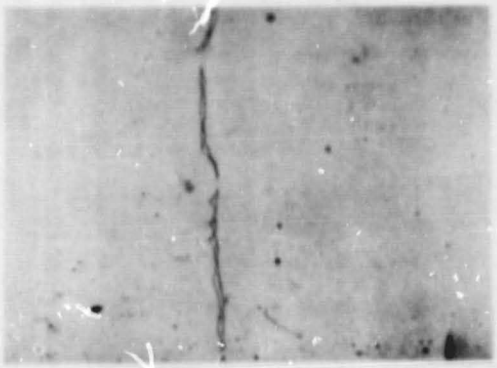

b) Metallographic, x 200

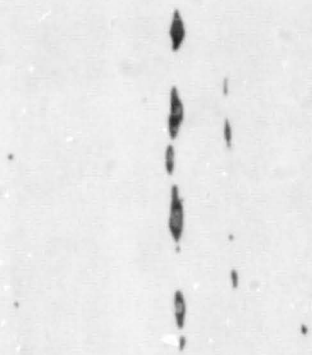

c) Metallographic, x 200

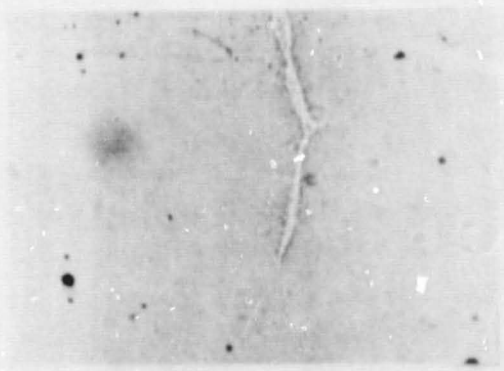

d) Metallographic, x 900

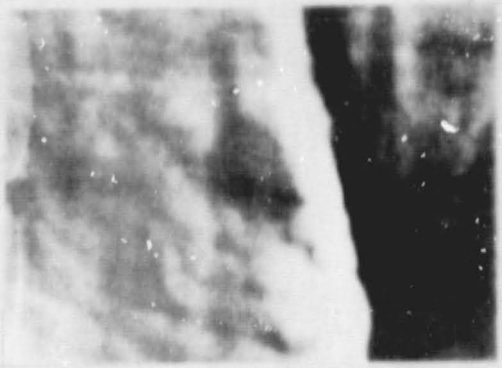

e) Microprobe, x 4750, Scanning Electron Image.

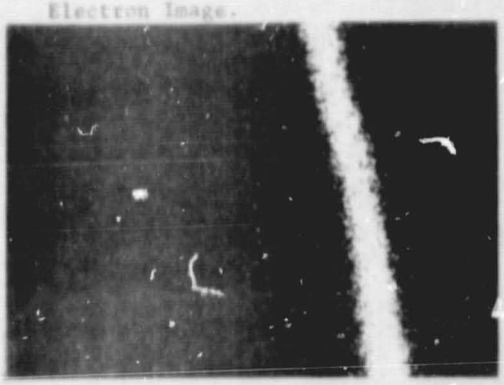

f) Microprobe, x 4750, Copper X-ray

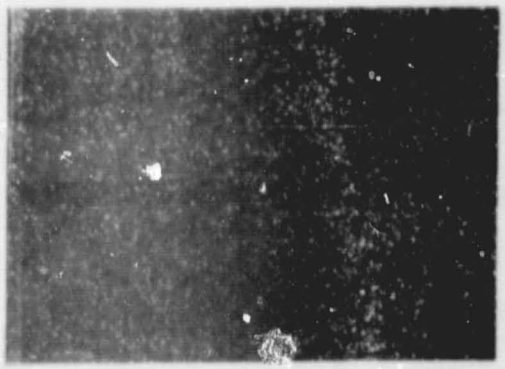

g) Microprobe, x 4750, Manganese X-ray

h) Microprobe, x 4750, Nickel X-ray

FIG.8: NITRONIC 40 STAINLESS STEEL, 300K, 60° BEND ON POLISHED SURFACE

a) Stereoscan, x 20 (edge crack)

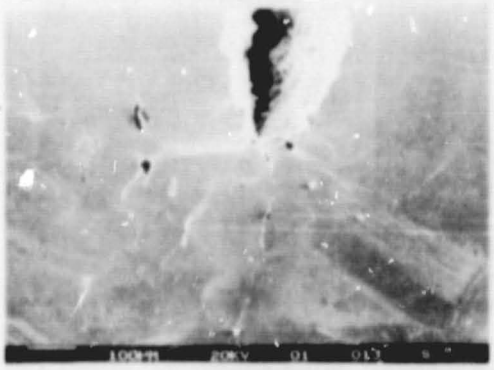

b) Stereoscan, x 80 (edge crack)

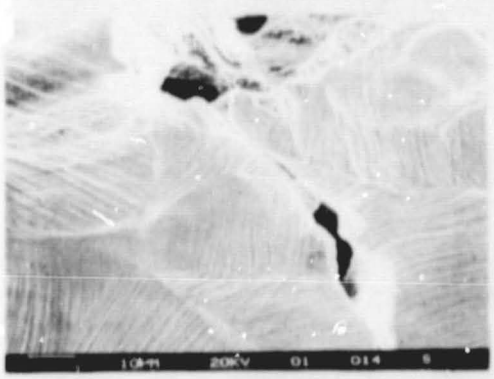

c) Stereoscan, x 800 (edge crack)

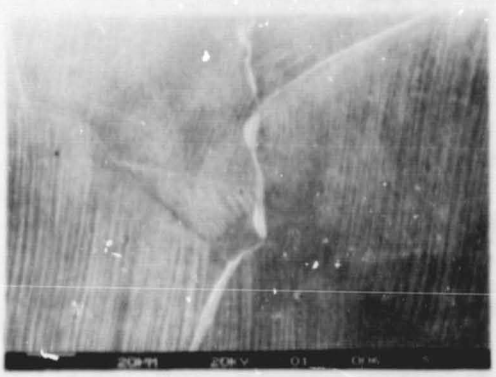

f) Stereoscan, x 400 (bond line)

d) Stereoscan, x 200 (internal crack)

g) Stereoscan, x 800 (bond line)

e) Stereoscan, x 400 (internal crack)

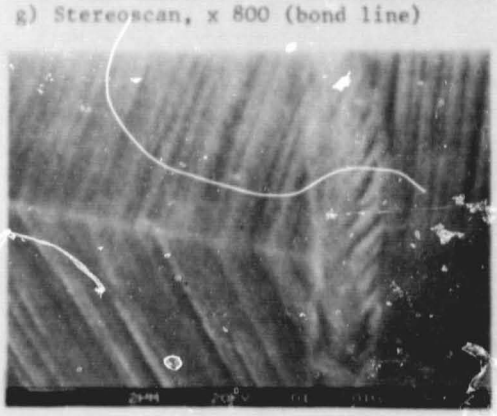

h) Stereoscan, x 4000 (bond line)

FIG.9: NITRONIC 40 STAINLESS STEEL, 300K, 3Pt BEND FRACTURE SURFACE

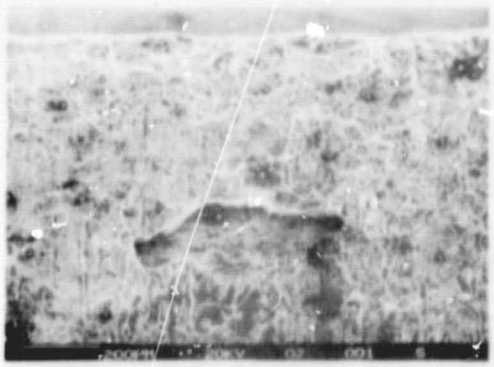

a) Stereoscan, x 60 (pull out)

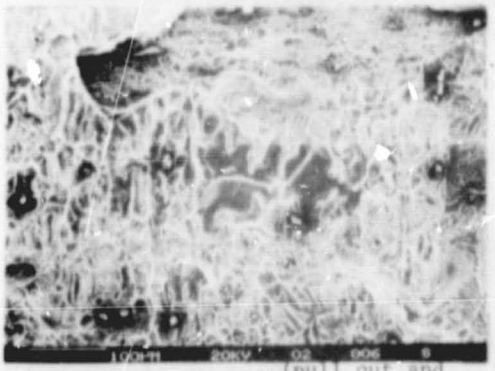

b) Stereoscan, x 120 (pull out and unwetted)

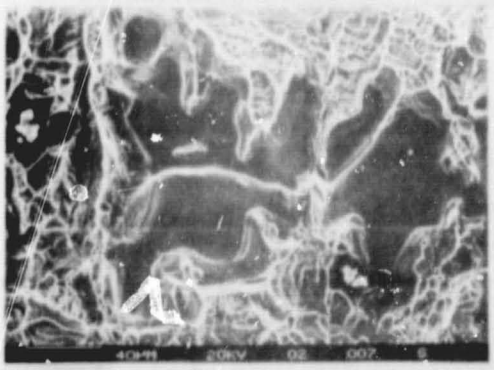

c) Stereoscan, x 300 (unwetted)

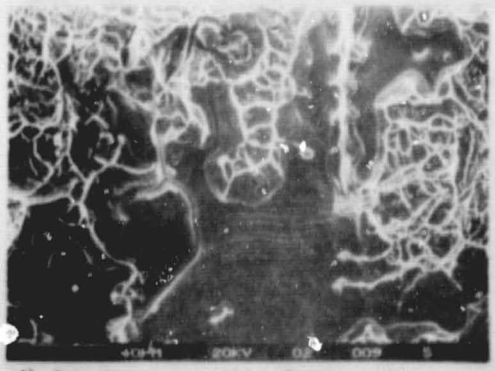

d) Stereoscan, x 300 (unwetted)

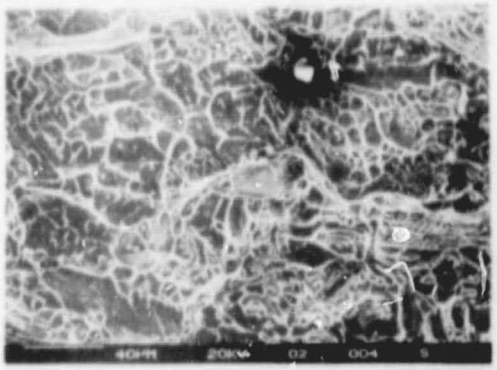

e) Stereoscan, x 300 (bond line)

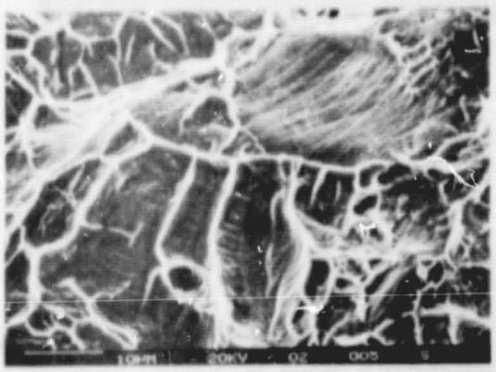

f) Stereoscan, x 1200 (bond line)

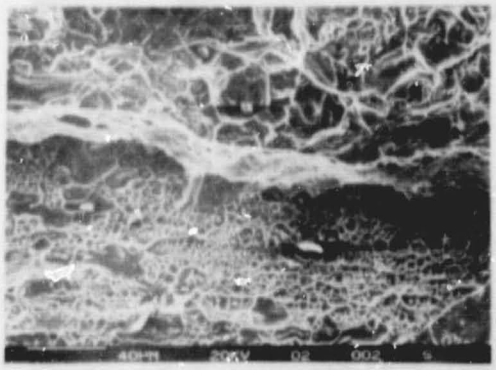

g) Stereoscan, x 300 (parent metal)

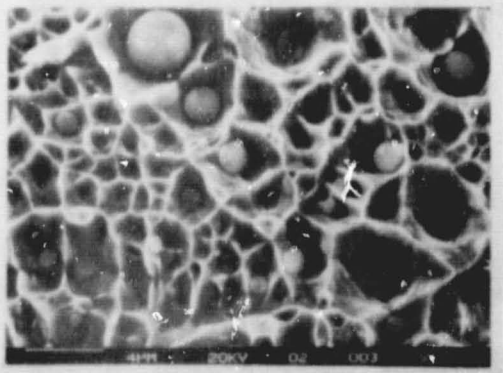

h) Stereoscan, x 3000 (parent metal)

FIG.10: NITRONIC 40 STAINLESS STEEL, 77K, CHARPY IMPACT FRACTURE SURFACE

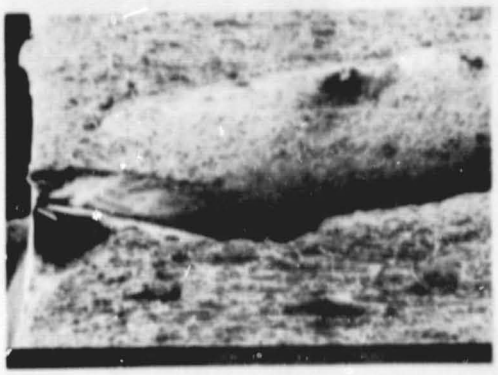

a) Stereoscan, x 14

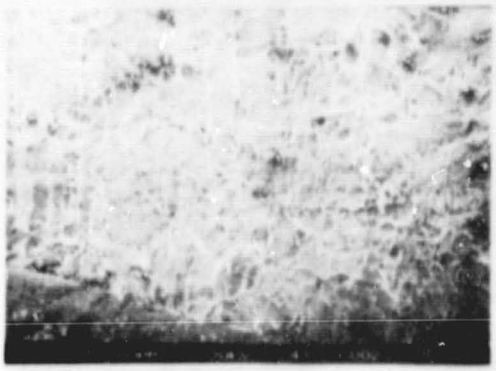

b) Stereoscan, x 70

c) Stereoscan, x 350

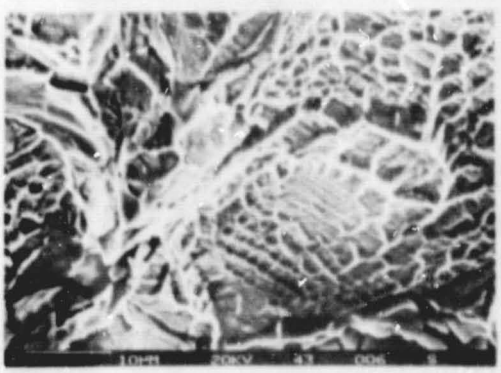

d) Stereoscan, x 1400

e) Stereoscan, x 350 (2nd area)

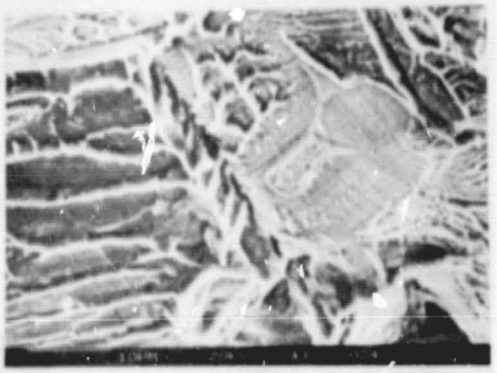

f) Stereoscan, x 1400 (2nd area)

g) Stereoscan, x 350 (inclusions)

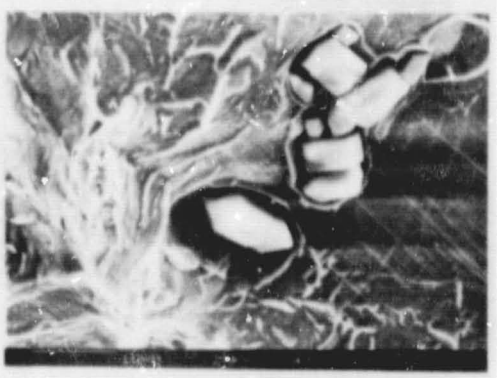

h) Stereoscan, x 1400 (inclusions)

FIG.11: CHARPY IMPACT FRACTURE SURFACES, 300K AND 77K

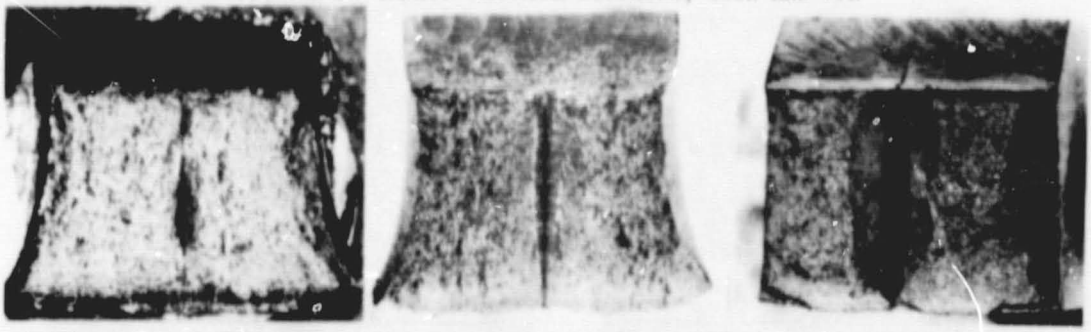

a) Nitronic 40, T1, 300K

e) 347, T1, 300K

i) 15/5 PH, T1, 300K

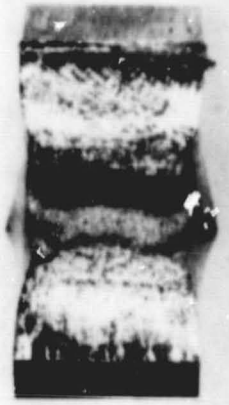

b) Nitronic 40, S2, 300K

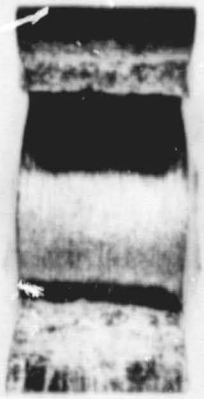

f) 347, S2, 300K

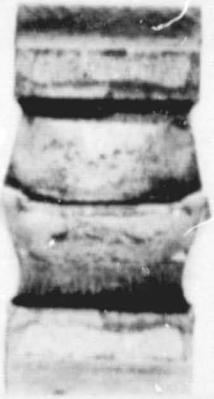

j) 15/5 PH, S2, 300K

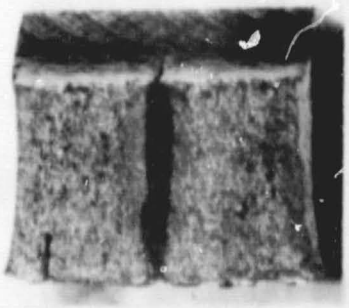

c) Nitronic 40, T3, 77K

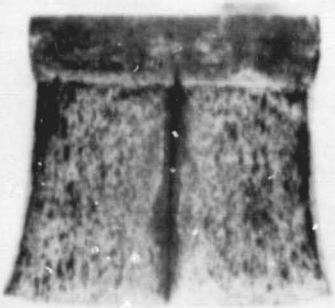

g) 347, T3, 77K

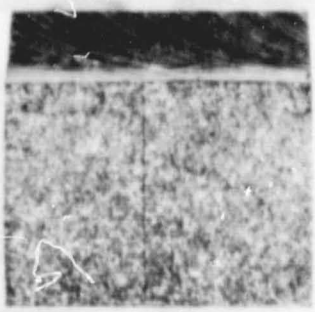

k) 15/5 PH, T3, 77K

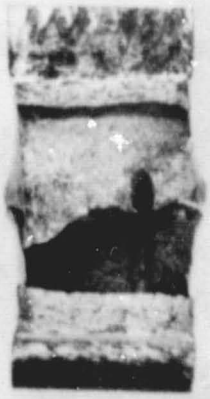

d) Nitronic 40, S4, 77K

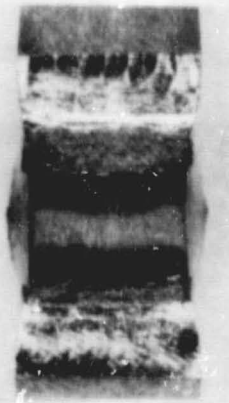

h) 347, S4, 77K

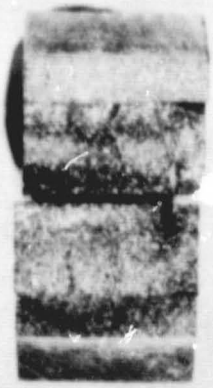

l) 15/5 PH, S4, 77K